

## *Ab initio* based description of the unusual increase of the electric field gradient with temperature at Ti sites in rutile TiO<sub>2</sub>

A. V. Nikolaev<sup>1,2,3</sup>, N. M. Chtchelkatchev<sup>4,3</sup>, A. V. Bibikov<sup>1,2</sup>, D. A. Salamatin<sup>5,6</sup> and A. V. Tsvyashchenko<sup>5</sup>

<sup>1</sup>Skobel'syn Institute of Nuclear Physics, Lomonosov Moscow State University, 119991 Moscow, Russia

<sup>2</sup>National Research Nuclear University MEPhI, 115409, Kashirskoe shosse 31, Moscow, Russia

<sup>3</sup>Moscow Institute of Physics and Technology, 141700, Dolgoprudny, Moscow Region, Russia

<sup>4</sup>Vereshchagin Institute for High Pressure Physics, Russian Academy of Sciences, 108840 Troitsk, Moscow, Russia

<sup>5</sup>Vereshchagin Institute for High Pressure Physics, RAS, 142190 Troitsk, Moscow, Russia

<sup>6</sup>Dzelepov Laboratory of Nuclear Problems, Joint Institute for Nuclear Research, 141980 Dubna, Russia



(Received 12 August 2020; revised 12 October 2020; accepted 29 October 2020; published 9 November 2020)

Combining a precise *ab initio* electron band structure calculation of the TiO<sub>2</sub> rutile structure with the temperature evolution of the Ti mean-square displacements, we reproduce a puzzling temperature increase of the electric field gradient at Ti sites in TiO<sub>2</sub>, observed experimentally. Our method employs a procedure of averaging two quadrupole electron density components ( $L = 2$ ) inside a sphere vibrating with the Ti nucleus at its center, where the key factor introducing the temperature dependence is the square root of the Debye-Waller factor. Although the Debye-Waller factor always reduces the corresponding Fourier component, in TiO<sub>2</sub> due to the interplay between terms of opposite signs, it results in a net increase of the whole sum with temperature, leading to the growth of the electric field gradient. Quantitatively, we find that the increase of electric field gradient is only half of the experimental value, which we ascribe to anharmonic effects or a strong oxygen position influence. In addition, our method reproduces the unusual temperature dependence of the asymmetry parameter  $\eta$ , which first decreases with temperature, goes to zero, and then increases.

DOI: [10.1103/PhysRevB.102.174305](https://doi.org/10.1103/PhysRevB.102.174305)

### I. INTRODUCTION

Nuclear spectroscopic methods, such as the time-differential perturbed angular correlation (TDPAC) technique and the Mössbauer spectroscopy, are very sensitive experimental instruments probing the local charge distributions of complex materials of interest over a wide temperature ( $T$ ) range [1–3]. These methods measure the electric field gradient (EFG) at nuclear probes [4,5], reflecting minute changes in their chemical environment and local bonding. In the case of a phase transition, EFG (or  $V_{zz}$ ) can change abruptly [6], but even without phase transitions the EFG demonstrates a smooth change with  $T$  [4,5]. Usually, this is a monotonic decrease with increasing  $T$ , very often in the functional form of  $V_{zz} \propto (1 - BT^{3/2})$  [4,7] (where  $B$  is a constant) but in some instances unexpectedly an increase of  $V_{zz}$  with  $T$  takes place. In particular, a weak increase of  $V_{zz}$  with  $T$  has been observed for the <sup>47</sup>Ti and <sup>49</sup>Ti nuclear probes in the rutile structure of titanium dioxide [8].

The nature of a strong temperature behavior of  $V_{zz}$  has been addressed in a number of theoretical and experimental research [4,5,9]. In principle, one can consider it as an anharmonic effect. Then, taking the experimental temperature dependence of lattice constants [ $a(T)$  and  $c(T)$  for TiO<sub>2</sub>, for example] and performing a set of EFG calculations at distinct values of  $a_i$  and  $c_i$  corresponding to various temperatures  $T_i$ , one can obtain the evolution of  $V_{zz}$  as a function of  $T$ . This is of course not a true *ab initio* approach, but even worse the

method in many cases does not work, giving wrong dependence: a decrease instead of increase and vice versa. This was realized already at the early stage of investigation albeit for a simple point charge model [4]. The challenge is to explain the temperature evolution of  $V_{zz}$  in the harmonic approximation, at least its general tendency to increase or decrease with  $T$ . To date there have been only a few attempts of such research [9,10].

A recent study [9] has combined an *ab initio* band structure approach with computing Debye-Waller factors (DWFs),  $\exp(-W(K, T))$  [11], to reproduce correctly the experimental temperature evolution of EFG in pristine metallic zinc and cadmium [7]. This method is in accord with early idea of Jena [12], who used a simple empirical model for the temperature dependence of DWFs and obtained a  $(1 - BT^{3/2})$  decrease of EFG. The model of Jena can only describe the reduction of  $V_{zz}$  with  $T$ , which seems logical taking into account the monotonic decrease of DWFs with temperature [11]. A fundamental question is as follows: Can the consideration based on DWFs explain an increase of EFGs, for example, in TiO<sub>2</sub>? As discussed in Ref. [9], in principle it is possible. However, it has been shown only that this type of behavior is not forbidden and can occur within a certain model dependence for the temperature evolution of mean-square displacements. In this paper, we extend the considerations developed in Ref. [9] to the rutile structure of TiO<sub>2</sub> and demonstrate that the method is capable of predicting the increase of  $V_{zz}$  with  $T$ .

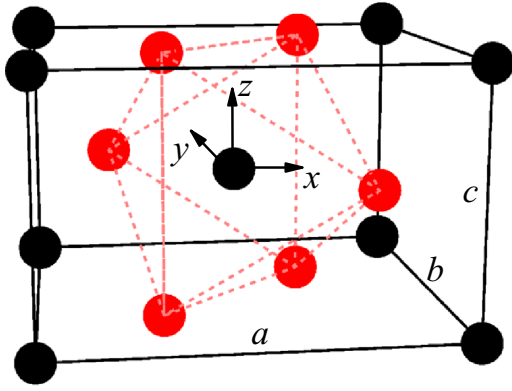


FIG. 1. Unit cell of the rutile phase of  $\text{TiO}_2$  and the Cartesian coordinate system (titanium, black spheres; oxygen, red spheres). The distorted oxygen octahedron around the central Ti atom is shown by red dashed lines. The lattice constants  $a$ ,  $b = a$ ,  $c$  are indicated.

The rutile phase of  $\text{TiO}_2$  is the thermodynamically stable form of the three known modifications (rutile, anatase, brookite) of titanium dioxide [13]. The Ti ions form the body-centered tetragonal structure, with each Ti ion surrounded by a distorted octahedron of six oxygen ions (Fig. 1). In the rutile unit cell there are two different Ti sites distinguished by two alternating orientations of the surrounded distorted oxygen octahedra. These octahedra and two tensors of electric field gradients at two Ti sites are related by a rotation through  $\pi$  about the  $z$  axis. Below in considering EFG tensor we refer to the central Ti site in Fig. 1.

The Ti-site EFGs have been measured with the native  $^{47}\text{Ti}$  and  $^{49}\text{Ti}$  nuclear probes by means of the nuclear magnetic resonance (NMR) spectroscopy [8]. These measurements performed on a single crystal over a large temperature range indicate that  $V_{zz}$  increases from  $2.11 \times 10^{21}$  V/m<sup>2</sup> at 150 K to  $2.86 \times 10^{21}$  V/m<sup>2</sup> at 1420 K. The second parameter  $\eta$ , the EFG asymmetry, starts from 0.2 at 300 K, goes to zero around 970 K, and then increases to 0.13 at 1420 K [8,14]. (The interpolated experimental plots for EFG and  $\eta$  are shown in Fig. 7 later.) In addition, the TDPAC spectroscopy has been applied to  $\text{TiO}_2$  to study EFG with the impurity  $^{111}\text{In} \rightarrow ^{111}\text{Cd}$  [15–17],  $^{181}\text{Hf} \rightarrow ^{181}\text{Ta}$  [16,18], and  $^{44}\text{Ti} \rightarrow ^{44}\text{Sc}$  [19,20] nuclear probes. The  $V_{zz}$  behavior of the  $^{111}\text{Cd}$  and  $^{181}\text{Ta}$  probes differs considerably from that of Ti. In contrast to  $^{181}\text{Ta}$  TDPAC measurements [16] showing as  $^{47,49}\text{Ti}$  an increase with  $T$ , the substitutional  $^{111}\text{Cd}$  probes result in a slow decrease of  $V_{zz}$  with  $T$  [16]. The room-temperature values of  $V_{zz}$  are  $13.4 \times 10^{21}$  V/m<sup>2</sup> for  $^{181}\text{Ta}$  and  $5.8 \times 10^{21}$  V/m<sup>2</sup>  $^{111}\text{Cd}$ . The asymmetry parameter  $\eta$  with these impurities also changes differently. In  $^{181}\text{Ta}$ ,  $\eta$  increases slightly from 0.57 at 300 K to 0.58 at 1300 K, whereas with  $^{111}\text{Cd}$ ,  $\eta$  changes from 0.2 at 300 K, goes to zero at 700 K, and then increases to 0.2 at 1300 K. Although recent TDPAC measurements of  $^{44}\text{Sc}$  probes in rutile modification of  $\text{TiO}_2$  found that EFG increased with  $T$  [20], they also showed a remarkable difference from the native  $^{47}\text{Ti}$  and  $^{49}\text{Ti}$  nuclear probes, detecting essentially  $T$ -independent antiaxial EFG with  $\eta = 0.94$  close to unity [19,20].

The EFG at Ti sites has been a subject of band structure investigations [17,21–23]. In the early study of Blaha *et al.*

[21] in pure  $\text{TiO}_2$  it has been found that in addition to valence states, there is a relatively large contribution to  $V_{zz}$  from the semicore Ti  $3p$  electron states, and that the value of  $V_{zz}$  is very sensitive to details of the electron band structure. In a series of first-principles calculations, the problem of a substitutional Cd impurity located at the Ti site has been addressed in Refs. [17,22,23]. On substituting the Ti atom by a Cd impurity, the *ab initio* calculation predicts strong anisotropic relaxations of the nearest oxygen neighbors and a change of the orientation of the largest EFG tensor component  $V_{33}$  from the (001) to the (110) direction [17]. To calculate the temperature dependence of  $V_{zz}$  at Cd the structural relaxation has been performed for a set of experimental temperature-dependent lattice constants  $a$  and  $c$  [23]. This study, however, refers to a decrease of  $V_{zz}$ .

To the best of our knowledge, no attempt was made to explain the temperature increase of  $V_{zz}$  in  $\text{TiO}_2$ . This issue is the main goal of this study. In Sec. II we briefly describe the method. Here, we generally follow the considerations of Ref. [9], but apply the approach to the problem of  $\text{TiO}_2$ . In Sec. III we present our results and discuss them. The conclusions are summarized in Sec. IV.

## II. THEORETICAL METHOD

### A. Electric field gradient in $\text{TiO}_2$

The EFG tensor  $V_{ij}$  is defined as the second partial spatial derivatives of the electric part of the self-consistent-field potential  $V(\vec{R})$  evaluated at the nuclear site, i.e.,

$$V_{ij} = \frac{\partial^2 V}{\partial i \partial j}, \quad (1)$$

where  $i = x, y, z$ .  $V_{ij}$ , being a symmetric second-rank tensor, can be further diagonalized by transforming coordinates to the principal system of axes ( $x', y', z'$ ) chosen such that  $|V_{z'z'}| \geq |V_{y'y'}| \geq |V_{x'x'}|$ . (Since  $V_{ij}$  is traceless, in the principal axis system the number of independent parameters for EFG is reduced to two.) The principal component ( $V_{z'z'}$ ) is called the electric field gradient, and the second independent parameter is the asymmetry  $\eta$  defined as  $\eta = (V_{x'x'} - V_{y'y'})/V_{z'z'}$  ( $0 \leq \eta \leq 1$ ).

It can be shown (see, e.g., Ref. [9]) that the EFG tensor  $V_{ij}$  is closely related to the quadrupole components ( $l = 2$ ) of the expansion of the electric part of the full potential  $V(\vec{R})$  in terms of the angular functions  $S_l^\tau(\theta, \phi)$ :

$$V(r, \theta, \phi) = \sum_{l, \tau} V_l^\tau(r) S_l^\tau(\theta, \phi). \quad (2)$$

Here,  $S_l^\tau(\theta, \phi)$  are the angular functions adapted for the rutile point crystal symmetry,  $l$  is the multipole orbital index, and  $\tau$  counts functions with the same  $l$  (if there are few such functions). The polar angles ( $\theta, \phi$ ) are specified by the vector  $\vec{r}$  from the closest nuclear position.  $S_l^\tau(\theta, \phi)$ , called symmetry-adapted functions (SAFs), are linear combinations of real spherical harmonics ( $Y_l^{m,c} \sim \cos m\phi$  and  $Y_l^{m,s} \sim \sin m\phi$ ) defined by the crystal site symmetry and tabulated in Ref. [24]. Equation (2) can be viewed as a standard expansion in terms of spherical harmonics, where each angular function has the full point crystal symmetry. Expansion (2) is a standard

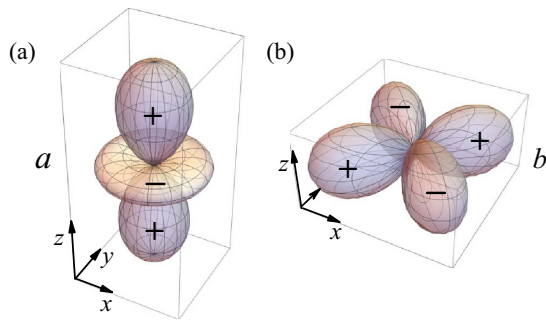


FIG. 2. Two angular quadrupole functions  $S_{Q,1}$  (a) and  $S_{Q,2}$  (b) [Eqs. (3a) and (3b)], used for the expansion of the electron density and electric potential at the titanium site in  $\text{TiO}_2$ . The  $x$ ,  $y$ , and  $z$  axes correspond to those shown in Fig. 1.

procedure in the full potential version of modern electron band structure codes [25].

At titanium site there are two quadrupole SAFs related to the EFG tensor (Fig. 2):

$$S_{Q,1}(\theta, \phi) = Y_{l=2}^0(\theta, \phi) \sim 3z^2 - r^2, \quad (3a)$$

$$S_{Q,2}(\theta, \phi) = Y_{l=2}^{2,s}(\theta, \phi) \sim xy. \quad (3b)$$

Here,  $Y_l^{m=0}$  and  $Y_l^{m,s}$  are real spherical harmonics with  $l = 2$ . Thus, the quadrupole part of the electric potential [Eq. (2)] is given by

$$V_Q(r, \theta, \phi) = V_{Q,1}(r)S_{Q,1}(\theta, \phi) + V_{Q,2}(r)S_{Q,2}(\theta, \phi). \quad (4)$$

Here,  $V_{Q,i}(r)$  ( $i = 1, 2$ ) are two independent radial components corresponding to the angular parts  $S_{Q,i}(\theta, \phi)$ . The EFG tensor  $V_{ij}$  [Eq. (1)] comes solely from the function  $V_Q$  [Eq. (4)], the contribution from the other terms in Eq. (2) is zero. As shown in Ref. [9], for the radial components  $V_{Q,i}(r)$  at  $r \rightarrow 0$  we obtain

$$V_{Q,1}(r) = v_{Q,1}r^2, \quad V_{Q,2}(r) = v_{Q,2}r^2, \quad (5)$$

where  $v_{Q,1}$  and  $v_{Q,2}$  are potential constants. The calculated dependencies of  $v_{Q,1}$  and  $v_{Q,2}$  on the lattice constant ratio  $c/a$  are shown in Fig. 3. From Eqs. (4) and (5) one can obtain the diagonal components of the EFG tensor

$$V_{11} = -v_{Q,1} \frac{1}{2} \sqrt{\frac{5}{\pi}} + v_{Q,2} \frac{1}{2} \sqrt{\frac{15}{\pi}}, \quad (6a)$$

$$V_{22} = -v_{Q,1} \frac{1}{2} \sqrt{\frac{5}{\pi}} - v_{Q,2} \frac{1}{2} \sqrt{\frac{15}{\pi}}, \quad (6b)$$

$$V_{33} = v_{Q,1} \sqrt{\frac{5}{\pi}}. \quad (6c)$$

Here, the diagonal component  $V_{11}$  is oriented along the (1,1,0) crystal lattice direction,  $V_{22}$  along the (-1, 1, 0) direction, and  $V_{33}$  along the (0,0,1) direction.

The calculated dependence of the components  $V_{jj}$  on the lattice constant ratio  $c/a$  with the fixed  $u = 0.3041$  is depicted in Fig. 4. From Figs. 3 and 4 (see also Sec. III) it follows that in  $\text{TiO}_2$  where  $c/a \approx 0.640$ – $0.644$ ,  $v_{Q,1} < 0$  and  $V_{zz} = V_{z'z'} = V_{33} < 0$  and hence  $V_{11} > 0$ ,  $V_{22} > 0$ . That is, the EFG value is associated with the  $V_{33}$  component along the (0,0,1) crystal lattice direction. For  $c/a < 0.641$   $v_{Q,2} < 0$ ,

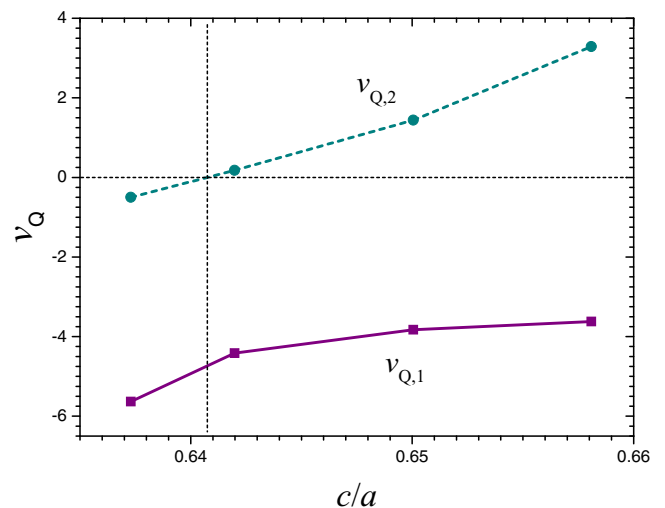


FIG. 3.  $v_{Q,1}$  and  $v_{Q,2}$  [Eq. (5)] versus the lattice constant ratio  $c/a$  (with  $u$  fixed) at  $T = 0$ , in units (eV/a.u.<sup>2</sup>). For  $c/a > 0.641$   $v_{Q,2} > 0$  and  $V_{11} > V_{22}$ , for  $c/a < 0.641$   $v_{Q,2} < 0$  and  $V_{11} < V_{22}$  [Eqs. (6a) and (6b)]. At  $c/a \approx 0.641$   $\eta = 0$ . (Calculations with the Moscow-FLAPW code, details are given in Sec. II C.)

$V_{11} < V_{22}$ , and  $V_{x'x'} = V_{11}$ ,  $V_{y'y'} = V_{22}$ ,  $\eta = (V_{11} - V_{22})/V_{33}$ . For  $c/a > 0.641$   $v_{Q,2} > 0$  and  $\eta = (V_{22} - V_{11})/V_{33}$  (Fig. 3).

Interestingly, at  $c/a > 0.653$  the largest diagonal component becomes  $V_{11}$  (i.e.,  $V_{z'z'} = V_{11}$ ) (Fig. 4). The change of  $V_{z'z'}$  orientation from (001) to (110) directions is experimentally observed for Cd probes in Ti sites in  $\text{TiO}_2$  [17,22], where it comes from the local anisotropic atomic relaxation introduced by the Cd impurity. In pure  $\text{TiO}_2$  the situation is different and the change of EFG is caused by the potential increase of  $c/a$  modifying the nearest neighbors' Ti-O relative distances

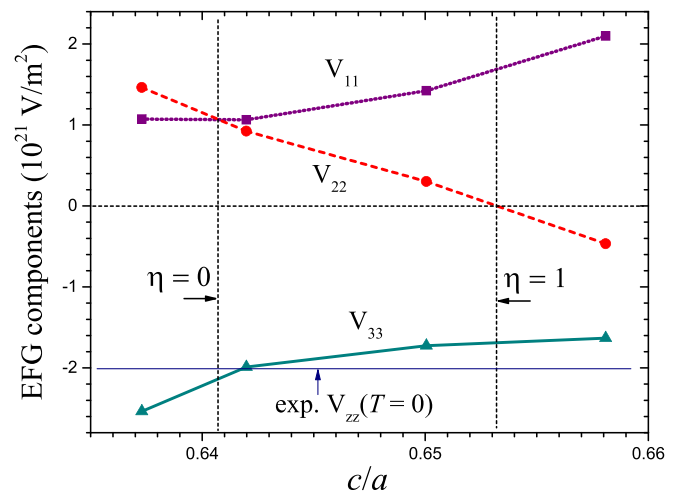


FIG. 4. Diagonal components  $V_{jj}$  ( $j = 1, 2, 3$ ) of the EFG tensor [Eqs. (6a)–(6c)] versus the lattice constant ratio  $c/a$  at  $T = 0$  (with  $u$  fixed). The electric field gradient  $V_{z'z'} = V_{33}$  for  $c/a < 0.653$ , and  $V_{z'z'} = V_{11}$  for  $c/a > 0.653$ . At  $c/a \approx 0.641$ ,  $\eta = 0$ , at  $c/a \approx 0.653$ ,  $\eta = 1$ . For comparison the  $T = 0$  value of  $V_{z'z'}$  obtained by the extrapolation of experimental data [8] is also shown. (Calculations with the Moscow-FLAPW code, details are given in Sec. II C.)

(those from the apical oxygens and those of the basal plane) and thus producing a similar effect.

Therefore, there are two critical points in Fig. 4. At  $c/a = 0.641$ ,  $\eta = 0$  and the EFG tensor is axial, whereas at  $c/a = 0.653$ ,  $\eta = 1$  and the EFG tensor is antiaxial [19].

### B. Temperature dependence of EFG

A general model for theoretical calculations of temperature dependence of EFG is presented in Ref. [9]. Here, we briefly outline it applying to  $\text{TiO}_2$  and working within the linear augmented plane-wave (LAPW) method [25].

The electron density around a nucleus being strongly coupled to it by the Coulomb interaction follows adiabatically the vibrating ion, while the electron density in the interstitial region interacting with several neighboring ions is less affected by the motion of a single atom. The dichotomy is resolved by considering vibrating spheres (muffin-tin or MT spheres) in the crystal with the electron density virtually unchanged in the interstitial region (between the spheres). That is, we assume that the Fourier expansion coefficients  $\rho(\vec{K})$  of the electron density in the interstitial density remain constant, and, following the procedure of LAPW method, calculate multipole density components on the vibrating MT spheres, which serve as the boundary surface conditions. Inside the MT spheres the electron density is expanded in terms of spherical harmonics. As shown in Ref. [9] at a finite and even zero temperature  $T$  the average quantities  $\langle\rho(\vec{K})\rangle$  on vibrating MT spheres are effectively reduced. In the language of the LAPW method, this implies a modification of boundary conditions for the solutions inside the MT spheres [25]. In particular, this procedure affects the average value of quadrupole components of electron density  $\langle\rho_Q\rangle$  associated with the multipole index  $l = 2$ . The change of  $\langle\rho_Q\rangle$  on the sphere surface (at  $r = R_{\text{MT}}$ ) translates inside it (i.e., at  $r \leq R_{\text{MT}}$ ) and finally leads to a change of EFG at  $r \rightarrow 0$ .

Unlike Ref. [9], the point symmetry of the Ti site in  $\text{TiO}_2$  supports two angular quadrupole functions  $S_{Q,i}$ ,  $i = 1, 2$  [Eqs. (3a) and (3b)], in the multipole expansions of the potential and electron density. Extending the considerations of Ref. [9], we then write for the average values of two quadrupole components of electron density on the Ti MT sphere,

$$\langle\rho_{Q,i}\rangle = -4\pi \sum_{\vec{K}} j_2(KR_{\text{MT}}) S_{Q,i}(\hat{K}) e^{-W(\vec{K},T)} \rho(\vec{K}). \quad (7)$$

Here, the summation is over the reciprocal vectors  $\vec{K}$ ,  $\hat{K}$  specifies the direction of  $\vec{K}$ , i.e.,  $\hat{K} \equiv (\theta_{\vec{K}}, \phi_{\vec{K}})$ ,  $j_2$  are spherical Bessel functions,  $S_{Q,1}$  and  $S_{Q,2}$  are the quadrupole SAFs given by Eqs. (3a) and (3b), and, finally,

$$W(\vec{K}, T) = \frac{1}{2} \langle (\vec{K} \cdot \vec{u})^2 \rangle, \quad (8)$$

where  $\vec{u}$  is the vector of the MT-sphere displacement. In Eq. (7), the effective reductions of  $\langle\rho(\vec{K})\rangle$  are described by the temperature function  $\exp(-W)$ , which is the square root of the Debye-Waller factor (SRDWF). [The conventional Debye-Waller factor is  $\exp(-2W)$  [11].] Earlier, SRDWF has been used by Kasowski in explaining the temperature-dependent Knight shift in cadmium [26,27].

As argued in Ref. [9] in a first approximation one can use an  $r$ -independent change (often reduction) of the quadrupole electron density component  $\rho_{Q,i}(r)$  inside the Ti MT sphere ( $r \leq R_{\text{MT}}$ ),

$$\frac{\langle\rho_{Q,i}(r, T)\rangle}{\rho_{Q,i}(r, u=0)} = \frac{\langle\rho_{Q,i}(R_{\text{MT}}, T)\rangle}{\rho_{Q,i}(R_{\text{MT}}, u=0)} = R_i(T). \quad (9)$$

Here,  $\langle\rho_{Q,i}(r, T)\rangle$  is the  $i$ th averaged quadrupole value inside the sphere ( $i = 1, 2$ ), while  $\rho_{Q,i}(r, u=0)$  is the quadrupole component in the absence of displacements ( $u=0$ ). Note that  $\langle\rho_{Q,i}(R_{\text{MT}}, T)\rangle$  on the surface of Ti MT sphere can be calculated by means of Eq. (7). Combining Eqs. (7) and (9), we obtain  $R_1$  and  $R_2$  as functions of  $T$ . At  $T = 0$ ,  $R_i(T) \approx 1$ . [The deviations of  $R_i(T = 0)$  from one are due to the zero point vibrations.]

The temperature changes of  $\rho_{Q,i}$  inside the Ti MT-spheres described by Eq. (9) lead to the proportional changes of the quadrupole potential components, i.e.,  $V_{Q,i}(r, T) = R_i(T)V_{Q,i}(r)$  [9]. Equation (4) then reads as

$$V_Q(r, \Omega, T) = V_{Q,1}(r, T) S_{Q,1}(\Omega) + V_{Q,2}(r, T) S_{Q,2}(\Omega), \quad (10)$$

where  $\Omega = (\theta, \phi)$ . At  $r \rightarrow 0$  we obtain  $V_{Q,i}(r, T) = v_{Q,i}(T) r^2$  [compare with Eq. (5)] where we have introduced temperature-dependent functions

$$v_{Q,1}(T) = v_{Q,1} R_1(T), \quad v_{Q,2}(T) = v_{Q,2} R_2(T). \quad (11)$$

Then, the temperature dependence of three components of EFG [Eqs. (6a)–(6c)] is explicitly expressed as

$$V_{11}(T) = -R_1(T) \frac{v_{Q,1}}{2} \sqrt{\frac{5}{\pi}} + R_2(T) \frac{v_{Q,2}}{2} \sqrt{\frac{15}{\pi}}, \quad (12a)$$

$$V_{22}(T) = -R_1(T) \frac{v_{Q,1}}{2} \sqrt{\frac{5}{\pi}} - R_2(T) \frac{v_{Q,2}}{2} \sqrt{\frac{15}{\pi}}, \quad (12b)$$

$$V_{33}(T) = R_1(T) v_{Q,1} \sqrt{\frac{5}{\pi}}. \quad (12c)$$

As long as  $V_{33}$  remains the largest diagonal component (i.e.,  $V_{zz} = V_{33}$ ) we arrive at

$$V_{zz}(T) \approx R_1(T) V_{zz}, \quad (13)$$

where  $V_{zz}$  is the  $T = 0$  value of EFG. On the other hand, the asymmetry parameter  $\eta(T)$  depends on both  $v_{Q,1}(T)$  and  $v_{Q,2}(T)$ .

In the following we will work in this approximation and, therefore, the only quantities that we have to calculate are two ratios of quadrupole components on the surface of Ti MT sphere  $R_i(T)$ , which completely describe the temperature dependence of the EFG tensor Eqs. (12a)–(13).

### C. Technical details of calculations

Electron density functional calculations have been performed with the Moscow-FLAPWcode [28]. The code explicitly takes into account the nuclear size and the change of the potential and the wave function inside the nuclear region to obtain the electric field gradient accurately. In addition, the number of radial points inside the MT region has been increased to 3000 (for some runs 3500). The typical LAPW

basis-set cutoff parameter was  $R_{MT}K_{max}$  from 7.8 to 8 with the number of basis functions from 583 to 737 for various runs, a typical number of  $k$  points in the irreducible part of the Brillouin zone (BZ) was 840. We have used the tetrahedron method for the linear interpolation of energy between  $k$  points. For calculation of the exchange-correlation potential we have used the PBEsol variant [29] of the generalized-gradient approximation (GGA) within the density functional theory (DFT). The precise calculations of  $V_{zz}$  and  $\eta$  have been performed for a number of various lattice constants whose  $c/a$  ratios are shown in Figs. 3 and 4. The correct behavior of  $\eta$  with  $T$  has been obtained for the lattice constants  $a = 4.5685 \text{ \AA}$ ,  $c = 2.9115 \text{ \AA}$ ,  $u = 0.30414$  with the MT radii  $0.8731 \text{ \AA}$ . It was assumed that the semicore (Ti  $3p$ ) states followed adiabatically the nuclei vibrations and their contribution to the interstitial region and temperature dependence was not considered.

For the phonon part required for mean-square displacement calculations, we have used the pseudopotential method as implemented in QUANTUM ESPRESSO (QE) [30,31], with the PBEsol exchange-correlation functional [29] and PBEsol optimized norm conserving Vanderbilt pseudopotentials (ONCVSP) [32] from the ONCVSP library [33]. The integration over the BZ for the electron density of states has been performed on a  $24 \times 24 \times 12$  grid of  $k$  points, the plane-wave kinetic cutoff energy was 70 Ry. The lattice-dynamical calculations have been carried out within the density-functional perturbation theory (DFPT). Phonon dispersions have been computed using the interatomic force constants based on a  $6 \times 6 \times 4$   $k$ -point grid, with a  $48 \times 48 \times 24$  grid used to obtain the phonon densities of states and the mean-square displacements of titanium and oxygen.

In both cases, the thermal expansion of the unit cell has not been taken into account.

### III. RESULTS AND DISCUSSION

First, we note that both the expansion of the lattice and a slight increase of  $c/a$  with temperature (with the rate  $2.2 \times 10^{-6} \text{ K}^{-1}$  [34]) lead to a smooth decrease of the electric field gradient  $V_{zz} = V_{33}$  (Fig. 4) (around  $c/a = 0.64$ ). Thus, the effect of the increase of EFG observed experimentally [8] is highly nontrivial.

Our typical calculation of the temperature evolutions of the potential quadrupole quantities  $v_{Q,1}$  and  $v_{Q,2}$  [Eq. (5)] are shown in Fig. 5 (for  $c/a = 0.6373$ ). The increase of  $v_{Q,1}$  with  $T$  unambiguously results in increase of EFG [Eqs. (12c) and (13)]. Interestingly,  $|v_{Q,2}|$  decreases with  $T$  and crosses the zero value at 940 K, after which the sign of  $v_{Q,2}$  is reversed. From Eqs. (12a) and (12b) then it follows that at 940 K  $\eta = 0$ , in close correspondence with experimental observations [8].

The increase of EFG in  $\text{TiO}_2$  is a very stable effect. It is found in a very wide range of lattice constants and  $c/a$  ratios. The temperature evolution of  $v_{Q,2}$  on the other hand is very sensitive to details of calculations. We have found that at  $c/a < 0.641$   $|v_{Q,2}|$  decreases as shown in the lower panel of Fig. 5, but increases at  $c/a > 0.641$  (Fig. 3).

The principal mechanism of an increase of EFG has been discussed in Ref. [9]. Below we briefly discuss it for  $\text{TiO}_2$ . From Eqs. (13) and (9) it follows that

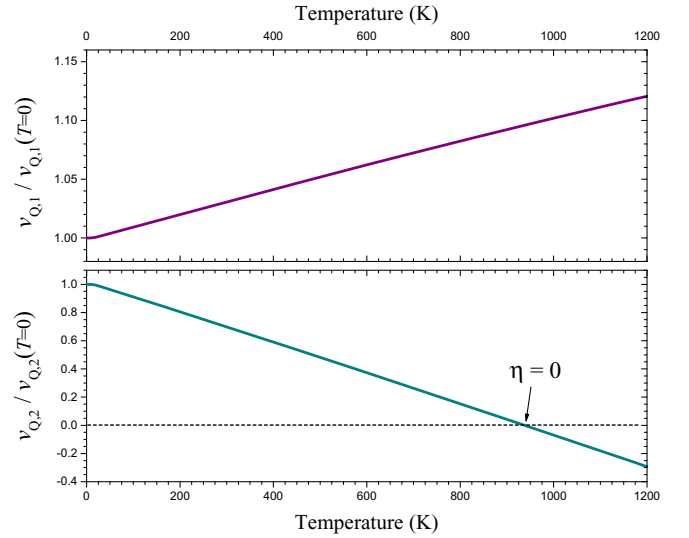


FIG. 5. Typical temperature dependencies of quadrupole parameters  $v_{Q,1}(T)/v_{Q,1}(0)$  and  $v_{Q,2}(T)/v_{Q,2}(0)$  [Eq. (11)] related to the quadrupole functions  $S_{Q,1}$  and  $S_{Q,2}$  [Eqs. (3a) and (3b)].

$V_{zz}(T) \propto \langle \rho_{Q,1}(R_{MT}, T) \rangle$ , while the Fourier expansion for  $\langle \rho_{Q,1}(R_{MT}, T) \rangle$  [Eq. (7)], being positive, can be further partitioned in two groups:

$$\langle \rho_{Q,1} \rangle = \sum_m |c_{1,m}| \mathcal{W}_{1,m}(T) - \sum_n |c_{2,n}| \mathcal{W}_{2,n}(T). \quad (14)$$

Here,  $\mathcal{W}_{i,p}(T) = \exp(-W(\vec{K}_{i,p}, T))$  ( $i = 1, p = m$  or  $i = 2, p = n$ ) are the temperature-dependent SRDW factors, while  $c_{i,p}(K_{i,p}) = -4\pi j_2(K_{i,p}R_{MT})S_{Q,i}(\vec{K}_{i,p})\rho(\vec{K}_{i,p})$  are temperature-independent coefficients, which can be positive or negative. [ $\rho(\vec{K}_{i,p})$  here are the Fourier coefficients entering also Eq. (7).] The difference between two explicitly written groups in Eq. (14) is that for all indices  $m$  and  $n$ ,  $c_{1,m} \geq 0$  whereas  $c_{2,n} < 0$ , and therefore, each of the two sums on the right-hand side of Eq. (14) is positive. While SRDWs  $\mathcal{W}_i$  and consequently the both sums always reduce with  $T$ , the whole sum for  $\text{TiO}_2$  increases. This occurs because the second sum in Eq. (14) drops fast enough to overcompensate the reduction of the first.

A detailed description of an increase of EFG is complicated: it clearly depends on the lattice structure through reciprocal vectors  $\vec{K}$  and connected with them numerical quantities  $c_{i,p}$  [expressed in  $j_2(K)$ ,  $S_{Q,i}(\vec{K})$ ], and also on the Fourier density components  $\rho(\vec{K})$ . All these quantities have been calculated numerically with the Moscow-FLAPW code [28]; details are given in Sec. II C. Other important quantities giving the explicit temperature dependence in SRDWs are mean-square displacements  $\langle u^2 \rangle$  of titanium [Eq. (8)]. In the case of the rutile phase of  $\text{TiO}_2$  there are three independent quantities:  $U_{11} = \langle u_x^2 \rangle$ ,  $U_{12} = \langle u_x u_y \rangle$ , and  $U_{33} = \langle u_z^2 \rangle$ , since by symmetry  $U_{22} = U_{11}$  and  $U_{13} = U_{23} = 0$ . Then,  $W(\vec{K}, T)$  [Eq. (8)] reads as

$$W(\vec{K}, T) = \frac{1}{2}[(K_x^2 + K_y^2)U_{11}(T) + 2K_x K_y U_{12} + K_z^2 U_{33}(T)]. \quad (15a)$$

TABLE I. Experimental mean-square displacements (in units  $10^{-3} \times \text{\AA}^2$ ) of titanium in  $\text{TiO}_2$ .  $U_{1'1'}$ ,  $U_{2'2'}$ , and  $U_{3'3'} = U_{33}$  are the diagonal values of the Ti thermal ellipsoid in principal axes. r.t. stands for the room temperature.  $U_{12} > 0$  in correspondence with the chosen coordinate axes (Fig. 1). The asterisk denotes MSDs converted from  $\beta_{11}$ ,  $\beta_{33}$ ,  $\beta_{12}$ .

Ref. $T$	$U_{11}$	$U_{12}$	$U_{1'1'}$	$U_{2'2'}$	$U_{33}$
[35] 15 K	1.2	0.2	1.0	1.4	1.1
[35] 295 K	5.5	0.3	5.2	5.8	4.5
[37] r.t.	6.8	0.4	6.4	7.2	4.6
[38] r.t.	6.68	0.12	6.56	6.80	4.81
[39] r.t.	6.9	0.0	6.9	6.9	4.4
[40]* 298 K	6.41	0.11	6.30	6.52	4.04
[41] 299 K	6.99	0.31	6.68	7.30	4.67
[34]* 298 K	7.64	0.06	7.58	7.70	4.21

It can be brought in the diagonal form

$$W(\vec{K}, T) = \frac{1}{2} [K_x^2 U_{1'1'}(T) + K_y^2 U_{2'2'}(T) + K_z^2 U_{33}(T)]. \quad (15b)$$

Here,  $K_x$  and  $K_y$  are projections of  $\vec{K}$  on new diagonal crystallographic axes  $[1\bar{1}1]$  and  $[111]$ , while the third axis ( $z' = z$ ) remains unchanged, and  $U_{1'1'} = U_{11} - U_{12}$ ,  $U_{2'2'} = U_{11} + U_{12}$ . Notice, that due to our initial choice of crystallographic axes (Fig. 1), the diagonal axes  $x'$  and  $y'$  are interchanged in comparison with those in experimental Refs. [35–41] and, consequently,  $U_{12} > 0$ .

A precise calculation of the mean-square displacements  $U_{11}$ ,  $U_{12}$ , and  $U_{33}$  (or, alternatively,  $U_{1'1'}$ ,  $U_{2'2'}$ , and  $U_{33}$ ) is a formidable problem. Even experimental data obtained from fitting neutron and x-ray diffraction study of the rutile using both single-crystal and powder samples of  $\text{TiO}_2$  at room temperature are quite different (see Table I).

Almost all of these studies refer to the room-temperature values of mean-square displacements (MSDs). To the best of our knowledge, in the literature there is only one low-temperature (15 K) neutron powder diffraction investigation of  $\text{TiO}_2$  carried out by Burdett *et al.* [35], whose data are also quoted in Table I. With these two-point MSD data taken at 15 and 295 K [35] assuming the linear dependence in all temperature range, one can construct the temperature dependence of  $U_{11}(T)$ ,  $U_{12}(T)$ , and  $U_{33}(T)$ . We shall refer to this  $T$  dependence of MSDs as model 1. The EFG parameters obtained with these MSDs are depicted in Fig. 6.

We have also performed the DF perturbation calculation of lattice dynamics with the QE package, details of which are described in Sec. II C. The results are shown in Fig. 6, model 2. In units  $10^{-3} \times \text{\AA}^2$  for 15 K we have obtained  $U_{11} = 2.62$ ,  $U_{12} = 0.06$ ,  $U_{33} = 1.85$ , and for 300 K,  $U_{11} = 12.85$ ,  $U_{12} = 0.52$ ,  $U_{33} = 6.89$ . Although these MSDs lie far above the experimental data, they are close to other values computed within the harmonic approximation. This is demonstrated in the Supplemental Material [42] where we compare our phonon data with a representative PHONOPY [43] phonon calculation of  $\text{TiO}_2$  from the phonon database at Kyoto University [44]. Thus, the calculated values of MSD are significantly overestimated in comparison with experimental

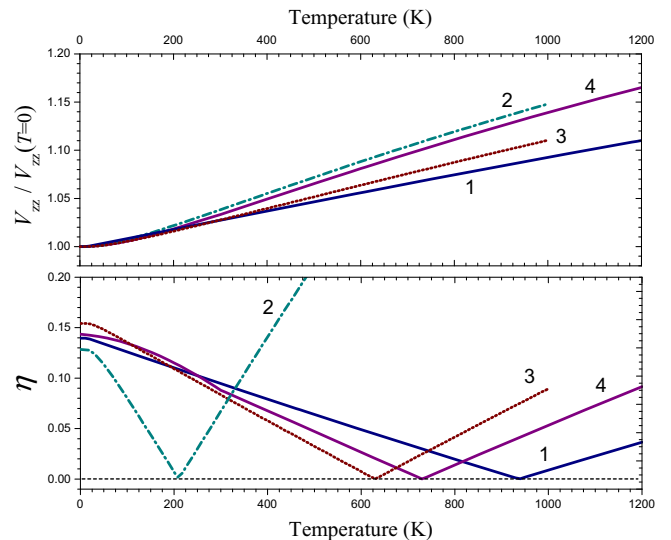


FIG. 6. Temperature evolution of  $V_{zz}$  and  $\eta$  calculated within four models for mean-square displacements ( $U_{11}$ ,  $U_{12}$ ,  $U_{33}$ ). Model 1: the linear approximation for MSDs with the values at  $T = 15$  and 295 K taken from Ref. [35]. Model 2: MSDs from the QE calculations (harmonic approximation). Model 3: the scaled MSDs from the QE calculations. Model 4: the modified Debye approximation ( $T_D = 600$  K [37]). Calculation with  $c/a = 0.6373$ .

ones (Table I). There are several reasons for this discrepancy. First, the harmonic calculation underestimates the experimental phonon energies [45]. In particular, the discrepancy reaches to nearly 5 meV for the low-lying transverse acoustic (TA) branch along the  $\Gamma$ -Z and  $M$ -Z directions [45]. Second, for the TA branch almost linear increase of phonon energies with temperature has been detected [45] which implies a stiffening of the entire TA branch with  $T$  [46]. In addition, in Refs. [45,46] a strong role of anharmonicity has been found with the phonon mode potential having strong positive fourth-order components, which leads to an increase of the phonon frequency for large atomic displacements occurring at higher temperatures. All these effects should result in a substantial decrease of MSDs calculated within the harmonic approximation at room temperature and above.

For a more realistic representation of the temperature evolution of MSD, we have scaled our QE data. The scaling factor has been chosen to fit the room-temperature MSD values of Ref. [38] (Table I). We refer to this  $T$  dependence of MSDs as model 3 (Fig. 6).

Finally, we can obtain the temperature dependence of MSDs using a modified Debye model. In Ref. [37] it has been shown that the model of isotropic vibrations of average amplitude with the Debye temperature  $T_D = 600$  K [37] fits the diffraction data. Within the Debye approximation we can calculate the average value of MSDs [ $U_{av} = (2U_{11} + U_{33})/3$ ]. We get  $U_{av} = 2.72 \times 10^{-3} \text{\AA}^2$  at 15 K and  $U_{av} = 6.00 \times 10^{-3} \text{\AA}^2$  at 300 K. Based on the  $T$  dependence of  $U_{av}$  and using the linear interpolation for the ratios  $U_{11}/U_{33}$  and  $U_{12}/U_{33}$  in the range from 15 to 300 K with the data of Ref. [35], we can obtain the anisotropic values of MSDs ( $U_{11}$ ,  $U_{12}$ ,  $U_{33}$ ) at all temperatures. This is the modified Debye model marked as model 4 in Fig. 6.

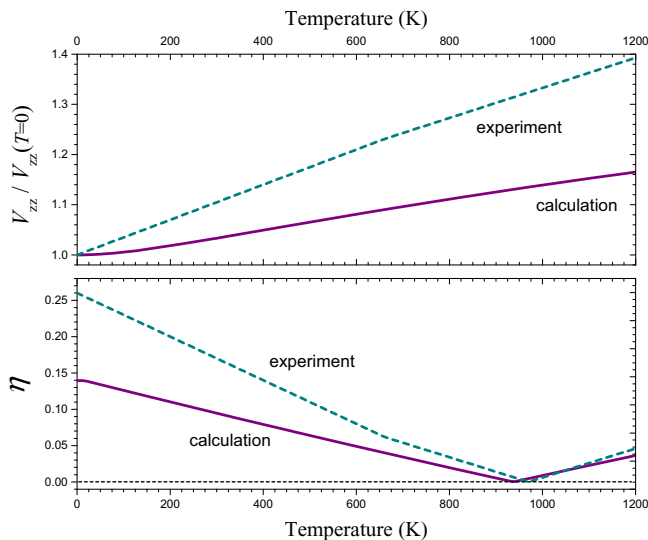


FIG. 7. Comparison with the NMR experimental data (Ref. [8]). The upper panel corresponds to the model 4, the lower panel to the model 1.

All four models for mean-square displacements result in a growth of EFG with temperature and a characteristic dependence of the asymmetry parameter  $\eta$  (Fig. 6). Numerically, the plots vary, reflecting a difference in the  $T$  evolution of mean-square displacements. In Fig. 7, the best calculated dependencies for EFG and  $\eta$  are compared with NMR data of Kanert and Kolem [8].

The theoretical increase of  $V_{zz}$  is approximately half of the experimental one. We ascribe it to anharmonic effects which were found important for the description of the temperature evolution of EFG in Zn and Cd [9]. EFG is found to be very sensitive to the correct temperature evolution of the ratio  $U_{33}(T)/U_{11}(T)$ , which could be the case for  $\text{TiO}_2$  taking into account a stiffening of its low-lying phonon energy spectrum with  $T$  and a strong fourth-order component of the potential [45,46]. Another important factor is a possible change of the oxygen rutile position  $u$  with  $T$ , which greatly influences the value of EFG [19].

The calculated  $V_{zz}$  is in good correspondence with the experimental value of  $2.0 \times 10^{21}$  V/m<sup>2</sup>, obtained by extrapolating experimental data to  $T = 0$  [8]. The zero-point vibrations lead to a 0.5% increase of the calculated EFG, to the corrected value  $1.998 \times 10^{21}$  V/m<sup>2</sup> at the experimental ratio  $c/a = 0.642$ .

#### IV. CONCLUSIONS

On the basis of *ab initio* calculations of the rutile phase of  $\text{TiO}_2$  we have reproduced qualitatively the temperature increase of the electric field gradient  $V_{zz}$  and the evolution of the asymmetry parameter  $\eta$  (Fig. 7). Note that if only the anisotropic thermal expansion of the lattice parameters is taken into account, i.e., an increase of  $c/a$ , this would predict a decrease of  $V_{zz}$ . Our consideration relies on the method used in Ref. [9] for calculation of the temperature dependence of EFG in Zn and Cd. The method utilizes the effect of changing the averaged value of the quadrupole components

( $\rho_{Q,1}$ ) and ( $\rho_{Q,2}$ ) [Eq. (7)] on a titanium MT sphere vibrating with the Ti nucleus. [The angular quadrupole functions  $S_{Q,1}$  and  $S_{Q,2}$  are explicitly given by Eqs. (3a) and (3b).] The temperature dependence is introduced through the factor  $\exp(-W(\vec{K}, T))$  which is the square root of the usual Debye-Waller factor [11], whereas the thermal expansion of the unit cell has not been taken into account. SRDWF effectively reduces the corresponding Fourier component of the electron density [Eq. (7)] and depends sensitively on the independent mean-square displacements  $U_{11}(T)$ ,  $U_{12}(T)$ , and  $U_{33}(T)$ .

$U_{11}(T)$ ,  $U_{12}(T)$ , and  $U_{33}(T)$  have been found experimentally (Table I) in neutron and x-ray diffraction studies at room temperature and at 15 K [35]. In addition, we have computed MSDs with QUANTUM ESPRESSO in the temperature range from 0 to 1000 K, but these values of  $U_{11}(T)$  and  $U_{33}(T)$  have turned out to be overestimated in comparison with the experimental ones. On the basis of experimental and calculated MSD data, we have adopted four models for their  $T$  dependence, and calculated corresponding  $V_{zz}(T)$  and  $\eta(T)$  (Fig. 6).

For all cases our results indicate a stable increase of EFG with temperature (Figs. 6 and 7). The increase of EFG is a remarkable effect arising from interplay of positive and negative terms [Eq. (14)]. While each term is reduced with temperature due to the  $\exp(-W(\vec{K}, T))$  factors, the whole sum can growth with  $T$ , leading to the increase of EFG. Quantitatively, however, the calculated growth of  $V_{zz}$  is smaller than the experimental one. This could be explained by an appreciable change of oxygen polarizability with  $T$  [19] or by anharmonic effects playing an important role in Zn and Cd [9]. Such effects include a nonlinear change of the  $U_{11}/U_{33}$  and  $U_{12}/U_{33}$  ratios with temperature, a change of oxygen position, and the thermal expansion of the rutile lattice. MSDs in  $\text{TiO}_2$  are apparently influenced by several unusual anharmonic effects [45–47] found in this compound.

For calculations with  $c/a < 0.641$  when  $V_{22} > V_{11}$  (Fig. 4), the calculated temperature evolution of  $\eta$  shows a good correspondence with experimental data (Figs. 7 and 6). In particular, it fairly well reproduces the crossing of the zero value, which is a nontrivial feature of the experimental curve [8]. This property is connected with the quadrupole potential parameter  $v_{Q,2}$  going through zero at this temperature (Fig. 5). For the  $c/a > 0.641$  case corresponding to the experimental  $c/a$  ratio,  $\eta$  demonstrates just a monotonic linear increase with  $T$  in disagreement with the experiment.

Interestingly, when  $c/a > 0.653$ , the electric field gradient switches to another component  $V_{z'z'} = V_{11}$  in Fig. 4. Note that such a situation is experimentally observed for Cd probes in  $\text{TiO}_2$  where it is accounted for by local displacements caused by Cd replacing a Ti atom in the rutile lattice [17,22]. Although the electronic configurations of Ti and Cd are quite different, the change in the orientation of  $V_{z'z'}$  from (001) to (110) is produced by a similar distortion of the nearest-neighbor oxygen octahedron.

#### ACKNOWLEDGMENTS

This research was supported by a grant of the Russian Science Foundation (Grant No. 18-12-00438). We are grateful

to the Polish representative at the Joint Institute for Nuclear Research. The numerical computations have been carried out using computing resources of the federal collective usage center Complex for Simulation and Data Processing for

Mega-science Facilities at NRC “Kurchatov Institute” [48] and supercomputers at Joint Supercomputer Center of RAS (JSCC RAS). We also thank the Uran supercomputer of IMM UB RAS for access.

- 
- [1] *Handbook of Applied Solid State Spectroscopy*, edited by D. R. Vij (Springer, New York, 2006).
- [2] T. Wichert and E. Recknagel, Perturbed Angular Correlation, in *Microscopic Methods in Metals. Topics in Current Physics*, edited by U. Gonser (Springer, Berlin, 1986), Vol. 40.
- [3] J. Schell, D. Zyabkin, D. C. Lupascu, Hans-Christian Hofsäss, M. O. Karabasov, A. Welker, and P. Schaaf, *AIP Adv.* **9**, 085208 (2019).
- [4] E. N. Kaufmann and R. J. Vianden, *Rev. Mod. Phys.* **51**, 161 (1979).
- [5] H. Haas, *Hyperfine Interact.* **129**, 493 (2000).
- [6] A. V. Tsvyashchenko, D. A. Salamatin, V. A. Sidorov, A. E. Petrova, L. N. Fomicheva, S. E. Kichanov, A. V. Salamatin, A. Velichkov, D. R. Kozlenko, A. V. Nikolaev, G. K. Ryasny, O. L. Makarova, D. Menzel, and M. Budzynski, *Phys. Rev. B* **92**, 104426 (2015).
- [7] J. Christiansen, P. Heubes, R. Keitel, W. Klinger, W. Loeffler, W. Sandner, and W. Withuhn, *Z. Phys. B* **24**, 177 (1976).
- [8] O. Kanert and H. Kolem, *J. Phys. C: Solid State Phys.* **21**, 3909 (1988).
- [9] A. V. Nikolaev, N. M. Chtchelkatchev, D. A. Salamatin, and A. V. Tsvyashchenko, *Phys. Rev. B* **101**, 064310 (2020).
- [10] D. Torumba, K. Parlinski, M. Rots, and S. Cottenier, *Phys. Rev. B* **74**, 144304 (2006).
- [11] P. Brüesch, *Phonons: Theory and Experiments II* (Springer, Berlin, 1986).
- [12] P. Jena, *Phys. Rev. Lett.* **36**, 418 (1976).
- [13] F. A. Grant, *Rev. Mod. Phys.* **31**, 646 (1959).
- [14] T. Butz, *Hyperfine Interact.* **198**, 161 (2010).
- [15] T. Wenzel, A. Bartos, K. P. Lieb, M. Uhrmacher, and D. Wiarda, *Ann. Phys. (Leipzig)* **504**, 155 (1992).
- [16] J. M. Adams and G. L. Catchen, *Phys. Rev. B* **50**, 1264 (1994).
- [17] L. A. Errico, G. Fabricius, M. Rentería, P. de la Presa, and M. Forker, *Phys. Rev. Lett.* **89**, 055503 (2002).
- [18] G. N. Darriba, L. A. Errico, P. D. Eversheim, G. Fabricius, and M. Rentería, *Phys. Rev. B* **79**, 115213 (2009).
- [19] S. B. Ryu, S. K. Das, T. Butz, W. Schmitz, C. Spiel, P. Blaha, and K. Schwarz, *Phys. Rev. B* **77**, 094124 (2008).
- [20] T. Butz and R. Vianden, *Hyperfine Interact.* **221**, 99 (2013).
- [21] P. Dufek, P. Blaha, and K. Schwarz, *Phys. Rev. Lett.* **75**, 3545 (1995); P. Blaha, D. J. Singh, P. I. Sorantin, and K. Schwarz, *Phys. Rev. B* **46**, 1321 (1992).
- [22] L. A. Errico, G. Fabricius, and M. Rentería, *Phys. Rev. B* **67**, 144104 (2003).
- [23] L. A. Errico, *Hyperfine Interact.* **158**, 29 (2004).
- [24] C. J. Bradley and A. P. Cracknell, *The Mathematical Theory of Symmetry in Solids* (Clarendon Press, Oxford, 1972).
- [25] D. J. Singh and L. Nordström, *Planewaves, Pseudopotentials, and the LAPW Method*, 2nd ed. (Springer, New York, 2006).
- [26] R. V. Kasowski and L. M. Falicov, *Phys. Rev. Lett.* **22**, 1001 (1969).
- [27] R. V. Kasowski, *Phys. Rev.* **187**, 891 (1969).
- [28] A. V. Nikolaev, D. Lamoën, and B. Partoens, *J. Chem. Phys.* **145**, 014101 (2016).
- [29] J. P. Perdew, A. Ruzsinszky, G. I. Csonka, O. A. Vydrov, G. E. Scuseria, L. A. Constantin, X. Zhou, and K. Burke, *Phys. Rev. Lett.* **100**, 136406 (2008).
- [30] P. Giannozzi, S. Baroni, N. Bonini, M. Calandra, R. Car, C. Cavazzoni, D. Ceresoli, G. L. Chiarotti, M. Cococcioni, I. Dabo, A. Dal Corso, S. Fabris, G. Fratesi, S. de Gironcoli, R. Gebauer, U. Gerstmann, C. Gougoussis, A. Kokalj, M. Lazzeri, L. Martin-Samos *et al.*, *J. Phys.: Condens. Matter* **21**, 395502 (2009).
- [31] P. Giannozzi, O. Andreussi, T. Brumme, O. Bunau, M. Buongiorno Nardelli, M. Calandra, R. Car, C. Cavazzoni, D. Ceresoli, M. Cococcioni, N. Colonna, I. Carnimeo, A. Dal Corso, S. de Gironcoli, P. Delugas, R. A. DiStasio Jr, A. Ferretti, A. Floris, G. Fratesi, G. Fugallo *et al.*, *J. Phys.: Condens. Matter* **29**, 465901 (2017).
- [32] D. R. Hamann, *Phys. Rev. B* **88**, 085117 (2013).
- [33] Available at [www.mat-simresearch.com](http://www.mat-simresearch.com).
- [34] K. Sugiyama and Y. Takéuchi, *Z. Kristallogr.* **194**, 305 (1991).
- [35] J. K. Burdett, T. Hughbanks, G. J. Miller, J. W. Jr. Richardson, J. V. Smith, *J. Am. Chem. Soc.* **109**, 3639 (1987).
- [36] R. J. Hill and C. J. Howard, *J. Appl. Crystallogr.* **20**, 467 (1987).
- [37] C. J. Howard, T. M. Sabine, and F. Dickson, *Acta Crystallogr. B* **47**, 462 (1991).
- [38] W. Gonschorek, *Z. Kristallogr.* **160**, 187 (1982).
- [39] W. Gonschorek and R. Feld, *Z. Kristallogr.* **161**, 1 (1982).
- [40] S. C. Abrahams and J. L. Bernstein, *J. Chem. Phys.* **55**, 3206 (1971).
- [41] H. Shintani, S. Sato, and Y. Saito, *Acta Crystallogr. B* **31**, 1981 (1975).
- [42] See Supplemental Material at <http://link.aps.org/supplemental/10.1103/PhysRevB.102.174305> for comparison our phonon data with a representative phonon calculation of TiO<sub>2</sub>.
- [43] A. Togo and I. Tanaka, *Scr. Mater.* **108**, 1 (2015).
- [44] Materials id 2657 / TiO<sub>2</sub> / P4<sub>2</sub>/mnm (136), <http://phonondb.mtl.kyoto-u.ac.jp/ph20180417/d002/mp-2657.html>.
- [45] B. Wehinger, A. Bosak, and P. T. Jochym, *Phys. Rev. B* **93**, 014303 (2016).
- [46] T. Lan, C. W. Li, O. Hellman, D. S. Kim, J. A. Muñoz, H. Smith, D. L. Abernathy, and B. Fultz, *Phys. Rev. B* **92**, 054304 (2015).
- [47] R. Restori, D. Schwarzenbach, and J. R. Schneider, *Acta Crystallogr. B* **43**, 251 (1987).
- [48] See <http://ckp.nrcki.ru>.